

## Sol-gel synthesis of topological insulator bismuth selenide nanoparticles by using different solvents

M. Z. Manzoor<sup>a</sup>, Z. Batool<sup>a,\*</sup>, Y. Ali<sup>a</sup>, H. M. Khan<sup>a</sup>, M. Ismail<sup>b</sup>, D. Ahmad<sup>a</sup>, H. Ullah<sup>a</sup>, A. Nazir<sup>a</sup>, R. Imran<sup>a</sup>

<sup>a</sup>*Institute of Physics, The Islamia University of Bahawalpur*

<sup>b</sup>*Division of Electrical and Electronics Engineering, Dongguk University, Seoul - 04620 Republic of Korea*

This paper reports about the Sol-Gel synthesis of Bismuth Selenide ( $\text{Bi}_2\text{Se}_3$ ) nanoparticles by using different solvents (DMF, Ethanol and (DMF+Ethanol)) for their potential in topological insulators. Various characterization techniques: X-ray diffraction (XRD), Fourier Transform Infrared spectroscopy (FTIR), photoluminescence (PL), and scanning electron microscope (SEM) were used to characterize the nano-powder. To get valuable information about dielectric behavior, AC impedance and conductivity were studied. The XRD measurements of Bismuth Selenide proved the crystalline form and orthorhombic crystal structure. The grain size (G) of Bismuth Selenide prepared in different solvents e.g., DMF, Ethanol, DMF+ Ethanol were calculated at 68 nm, 78 nm, and 84 nm respectively. FTIR study showed that the wavenumber corresponding to  $660\text{-}800\text{cm}^{-1}$  represents the vibrational bands of Bismuth Selenide ( $\text{Bi}_2\text{Se}_3$ ). Photoluminescence analysis revealed that the maximum absorption was at 801 nm and the bandgap was approximately 1.7eV for all the solvents. The surface morphology of the synthesized Bismuth Selenide ( $\text{Bi}_2\text{Se}_3$ ) was studied with the help of a scanning electron microscope (SEM). The dielectric study showed the frequency effect on dielectric constant ( $\epsilon'$ ), dielectric loss ( $\epsilon''$ ), tangent loss ( $\tan\delta$ ), impedance (Z), and AC conductivity.

(Received February 19, 2022; Accepted May 30, 2022)

*Keywords: Sol-Gel,  $\text{Bi}_2\text{Se}_3$ , Topological insulator, AC impedance, Conductivity, Dielectric study*

### 1. Introduction

Topological Insulators are distinct from ordinary insulators as their interior has no conduction band (bulk band gap) because in the bulk there is an energy gap between the ground and 1<sup>st</sup> excited states of electrons similar to those of a conventional insulator, but at their boundaries electrons can move, and hence conduct charge, without paying an energy penalty. While possessing conductive or metallic surface state, [1-2] secured by time-reversal symmetry. [3]

Bismuth Selenide ( $\text{Bi}_2\text{Se}_3$ ) a member of the family of  $\text{A}^{\text{V}}\text{B}^{\text{VI}}$  semiconductor materials, is the exemplary topological insulator material. The discovery of a single Dirac cone [4] at the Brillion zone center in  $\text{Bi}_2\text{Se}_3$  has attracted to a greater extent the attention of the research community. It is also known as thermoelectric material with a relatively small bandgap approximately measured between 0.2-0.3 eV [5]. Hence,  $\text{Bi}_2\text{Se}_3$  is a model for probing investigations into the application of topological insulator material. Many investigators explore topological insulators theoretically [6–8] and experimentally [9-10] however it is still an underexplored field.

Topological insulators including  $\text{Bi}_2\text{Se}_3$ ,  $\text{Sb}_2\text{Te}_3$ , and  $\text{Bi}_2\text{Te}_3$  are 3-dimensional and show TIs manners at room temperature [11] and are often called second-generation materials. TI based materials exhibit attractive features in the field of spintronics, Hall effect, magnetometer, high-

---

\* Corresponding author: zahida.batool@iub.edu.pk  
<https://doi.org/10.15251/DJNB.2022.172.649>

frequency magnetic power sensor, humidity sensor and wideband radiation detector using the Seebeck and Peltier effects [12-15], electro-thermal cooling modules [16], infrared photography [17], photoelectrochemical cells, optical and photosensitive devices [18], field-effect transistor (FET), LASER, energy competent products and many other modern technologies. A fascinating fact about Topological insulators is their low-temperature superconductivity [19-20].

Mostly the investigator developed  $\text{Bi}_2\text{Se}_3$  crystals by a variety of techniques such as *Qiu et al.* [21] synthesized  $\text{Bi}_2\text{Se}_3$  nano-materials by sonochemical route using  $\text{Bi}(\text{NO}_3)_3$ , EDTA,  $\text{Na}_2\text{SeSO}_3$ , and ascorbic acid as precursor materials; *Cui et al.* [22-23] reported  $\text{Bi}_2\text{Se}_3$  nanobelts or nanotube via sonochemical method using  $\text{BiCl}_3$ , selenious acid and diamine hydrate as the starting materials, *Wang et al.* [24] synthesized  $\text{Bi}_2\text{Se}_3$  nanopowders by a solvothermal method by using ethylene-diamine (en) using  $\text{BiCl}_3$  and Selenium as starting materials and sodium iodide (NaI) as a reducing agent. Moreover, hydrothermal route, solid-state reaction method, self-flux method, solvothermal method (*Kadel et al.* (2011)), vapor-liquid-solid and melt growth method are also applicable for the fabrication of  $\text{Bi}_2\text{Se}_3$  crystals. [25-26].

We have successfully synthesized  $\text{Bi}_2\text{Se}_3$  NPs via the sol-gel method which is not reported in the literature until now. Bismuth nitrate pentahydrate and elemental selenium were used for manufacturing the NPs. Different types of solvents like ethanol and DMF and their combination were used in the fabrication of NPs to investigate which solvent exhibited the best results for the sol-gel technique. The structural and phase composition, surface morphology, optical properties and band analysis of the prepared nanopowder were characterized by XRD, SEM, PL, and FTIR respectively.

## 2. Experimental work

### 2.1. Materials and chemicals

Bismuth nitrate pentahydrate ( $\text{Bi}(\text{NO}_3)_3 \cdot 5\text{H}_2\text{O}$ ) and Elemental selenium (Se) (with 99.99% purity) purchased from *Sigma Aldrich*, Dimethylformamide (DMF), Ethanol ( $\text{C}_2\text{H}_5\text{OH}$ ), NaOH, Ammonia solution, Distilled/Deionized water.

### 2.2. Synthesis of $\text{Bi}_2\text{Se}_3$ NPs

Bismuth Selenide ( $\text{Bi}_2\text{Se}_3$ ) nanoparticles were synthesized via the Sol-gel route at  $90^\circ\text{C}$ . Bismuth nitrate pentahydrate ( $\text{Bi}(\text{NO}_3)_3 \cdot 5\text{H}_2\text{O}$ ) and elemental Selenium (Se) were dissolved successively in various solvents i.e. DMF, Ethanol and DMF & Ethanol combined solvent. An appropriate amount of NaOH or ammonia was introduced into the solution to regulate the pH of the mixture at 10. After a few hours, the black precipitates were developed and allowed to cool naturally, washed with distilled/deionized water, filtered, and dried in a vacuum. Finally, black-colored  $\text{Bi}_2\text{Se}_3$  NPs were obtained.

## 3. Results and discussion

### 3.1. Structural analysis by X-ray diffraction

To examine the structural composition and crystallography of Bismuth Selenide ( $\text{Bi}_2\text{Se}_3$ ) nanoparticles, the XRD technique was employed using  $\text{CuK}\alpha$  ( $\lambda=1.54178\text{\AA}$ ) radiation and the XRD pattern recorded for bismuth selenide nanopowder synthesized using different solvents is presented in Fig. 1 which is following JCPDS (01-077-2016). It is clear (from Fig. 1) Bismuth Selenide prepared in various solvents DMF, ethanol, and a mixture of DMF & absolute ethanol revealed a similar XRD pattern and mainly contain Bismuth Selenide ( $\text{Bi}_2\text{Se}_3$ ) with a small amount of Bismuth Oxide ( $\text{Bi}_2\text{O}_3$ ) phase [27-28].

The X-ray diffraction peaks of the materials in Fig. 1 proved the orthorhombic system of  $\text{Bi}_2\text{Se}_3$  space group 62-pbnm (with JCPDS (01-077-2016) with lattice parameter  $a=11.62\text{ \AA}$ ,  $b=11.83\text{ \AA}$  and  $c=4.20\text{ \AA}$ . No additional peaks were observed in the diffraction patterns confirming the formation of pure  $\text{Bi}_2\text{Se}_3$ . The plane (0 1 5) at Bragg's angle  $29.68^\circ$  exhibited strong diffraction

intensity which is the evidence for the preferred orientation of Bismuth Selenide ( $\text{Bi}_2\text{Se}_3$ ) along [0 1 5] direction. [24]

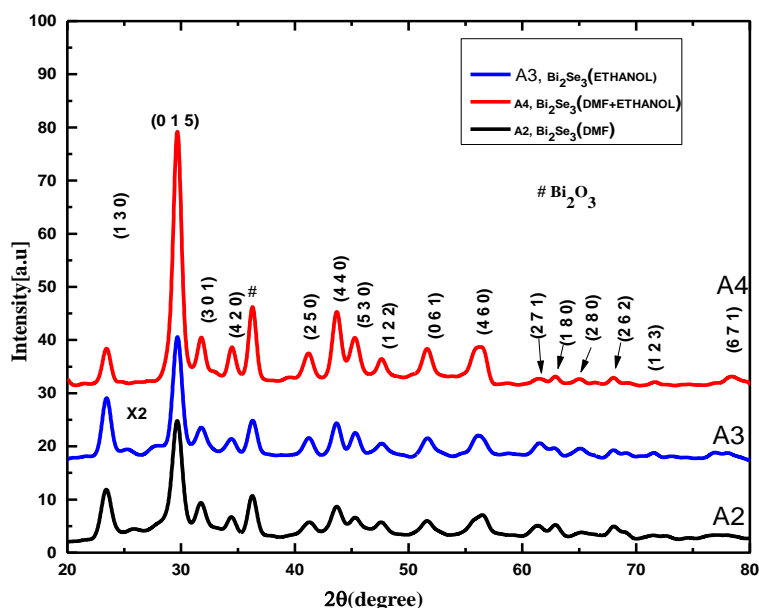


Fig. 1. XRD patterns of the products synthesized using various solvents.

One diffraction peak was observed at Bragg's angles  $36.3^\circ$  in all patterns in Fig.1, which didn't correspond with diffraction data given in JCPDS data (file no. 01-077-2016 and 53-61386). The observed peak corresponds to the Bismuth Oxide ( $\text{Bi}_2\text{O}_3$ ) phase or Bismuth Selenium oxide ( $\text{Bi}_2\text{O}_5\text{Se}$ ) that could also be formed during the synthesizing process [27-28]. The degree of purity of the material obtained is relatively high.

The gain size of Bismuth Selenide nanopowder was calculated by using Debye Scherer's formula:

$$G = \frac{k\lambda}{\beta \cos \theta} \quad (1)$$

where  $k = 0.9$  Scherrer constant,  $\lambda$  represent the wavelength of X-rays,  $\beta$  represents full width at half maximum and  $\theta$  represents Bragg's angle obtained from  $2\theta$  values corresponding to the peak in the XRD pattern.

According to Scherer's formula, the grain size ( $G$ ) of Bismuth Selenide prepared in different solvents e.g. DMF, DMF+ Ethanol, and Ethanol is 68 nm, 78 nm, and 84 nm respectively.

The grain size of Bismuth Selenide NPs prepared in a mixed solvent of DMF & Ethanol was larger. The larger size in mixed solvent is due to partial solubility of elemental selenium (Se) and bismuth (Bi) that remain non-reactive to some extent in these solvents [29]. In the mixed solvent of DMF & ethanol, each solvent was strongly bonded to each other than bismuth and selenide, so in this mixed solvent due to weak solubility, the grain size of nanopowders become larger relatively. The synthesized product generally contains elemental Bi and Se, with a little amount of  $\text{Bi}_4\text{Se}_3$  [29].

### 3.2. Optical studies

The photoluminescence absorption spectrum of Bismuth Selenide ( $\text{Bi}_2\text{Se}_3$ ) powder was recorded in the range between 300-1100 nm. The emission band of  $\text{Bi}_2\text{Se}_3$  powder shows a very smooth fitting of PL spectra. The peaks center appeared and recorded the bandgap in the range between 1.72 eV-1.75 eV in all samples. The bandgap of bismuth Selenide having a value of 1.72

eV was found to be smaller for the sample prepared in DMF + Ethanol solvent but the other sample had a slightly larger value approximately 1.75 eV consistent with grain size variations. The bandgap energy of  $\text{Bi}_2\text{Se}_3$  powder depends on the grain size and increases with a decrease in quantum size. The larger value of the bandgap in the present case is due to the quantum size effect [68]. The results show that the sample prepared in DMF solvent has the most intense and smooth peak (709) with the smallest line width value (0.17eV), which shows that the A2 sample has better efficiency of Photoluminescence. Another intense peak (138) corresponds to a sample prepared in a mixed solvent of DMF & ETHANOL whose PL intensity is smaller than that of the sample prepared in DMF solvent (709) but larger than the ETHANOL (123) sample. In the case of FWHM, the sample prepared in DMF solvent has a minimum FWHM value as compared to DMF+ETHANOL and ETHANOL prepared samples. The most intense peak and smallest FWHM value manifested that the sample prepared in DMF solvent has good Photoluminescence.

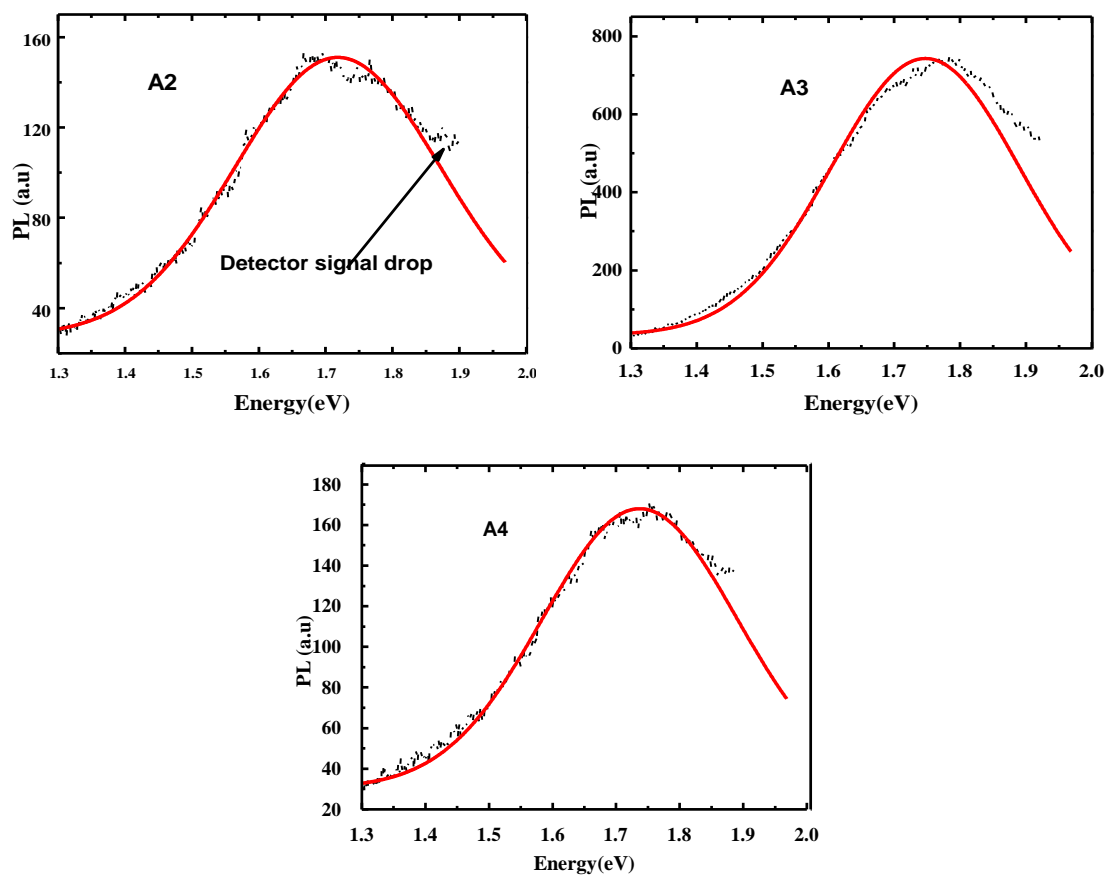


Fig. 2. A complete comparison of the PL absorption spectra for a bandgap of bismuth Selenide prepared in all solvents.

### 3. FTIR analysis

The FTIR spectrum of  $\text{Bi}_2\text{Se}_3$  is reported in the wavelength range from 800-600  $\text{cm}^{-1}$  using (SHIMADZU) spectrometer at the Institute of Physics in the Islamia University of Bahawalpur. The FTIR spectra of  $\text{Bi}_2\text{Se}_3$  as shown in Fig. 3, revealed the vibrational frequencies of the synthesized materials. Fig. 3 shows a complete comparison of evidence of the Bi-Se bond present in Bismuth Selenide nano-structured powder prepared in various solvents.

A prominent peak measured at 800-660  $\text{cm}^{-1}$  in all samples represents the existence of Bi-Se bond stretching vibrations [30]. The peaks corresponding to  $\text{Bi}_2\text{Se}_3$  stretching vibrations at 655  $\text{cm}^{-1}$  and 712  $\text{cm}^{-1}$  are in reasonable agreement with ref. [30]. The bands observed at 655  $\text{cm}^{-1}$  and 715  $\text{cm}^{-1}$  in the spectrum may be due to C=O, C=C and  $\text{NO}_2$  vibrations respectively [30].

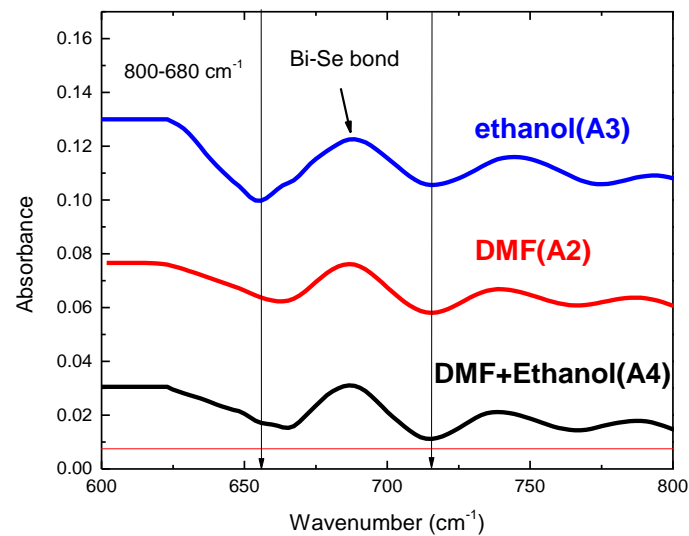


Fig. 3. Complete comparison of all FTIR spectra of Bismuth Selenide nanoparticles prepared in different solvents.

#### 4. Scanning Electron Microscopy (SEM)

Fig. 4 shows the surface morphology of the synthesized Bismuth Selenide ( $\text{Bi}_2\text{Se}_3$ ) with the help of a scanning electron microscope (SEM).

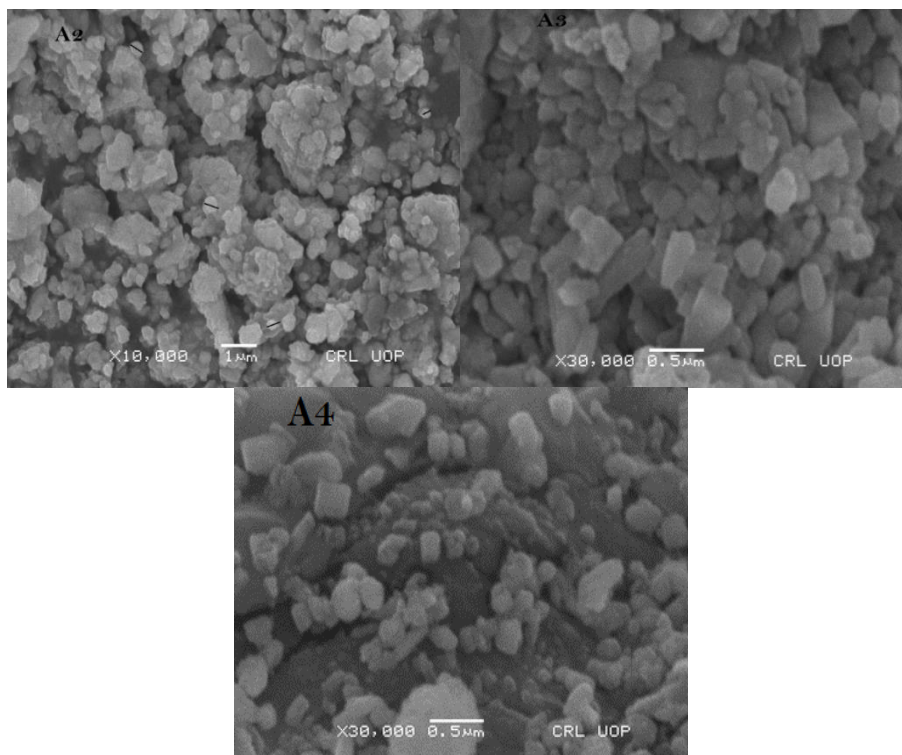


Fig. 4. Shows SEM images of Bismuth Selenide nanoparticles ( $\text{Bi}_2\text{Se}_3$ ).

These recorded micrographs showed that all samples resemble irregular sheet-like microcrystal morphology. At measurements scale to 0.5 μm (Fig. 4), the microphotographs of  $\text{Bi}_2\text{Se}_3$  appeared to be less agglomerated and show a nearly homogeneous allocation of particles. The SEM images of  $\text{Bi}_2\text{Se}_3$  nanoparticles are captured at different magnifications (i.e. at 0.5 μm, 1 μm, 5

$\mu\text{m}$ , and  $10\mu\text{m}$ ). It is important to declare that the grain size from SEM microphotographs seems to be in the nanoscale range.

## 5. Dielectric studies

### 5.1. Dielectric constant

The change in dielectric constant concerning frequency for Bismuth Selenide was measured in a frequency range from 10 Hz to 8 MHz at room temperature. The values of the dielectric constant ( $\epsilon'$ ) of  $\text{Bi}_2\text{Se}_3$  are in the range of frequencies from 1 kHz to 8 MHz. The variation of the dielectric constant concerning frequency is presented in Fig. 5

Dielectric constant ( $\epsilon'$ ) can be worked out by using the following relation: a

$$\epsilon' = \frac{\epsilon}{\epsilon_0} \quad (2)$$

where  $\epsilon$  denotes permittivity of medium and  $\epsilon_0$  denotes permittivity of vacuum and its value is  $8.85 \times 10^{-12}$  F/m. The graph of dielectric constant or permittivity shows that the value of dielectric permittivity decreases with the rise in frequency. Initially, the value of the Dielectric constant is higher at lower frequencies thereafter it comes down gradually and becomes almost stable with an increase in frequency. This revealed that at higher frequencies samples become highly effective for all samples.

The reason behind the large value of dielectric constant at low frequency may be primarily caused by the occurrence of polarizations (atomic, dipolar, ionic, and interface) for all samples. An increase in space charge polarization may be a result of a large concentration of defects. [31] As soon as frequency increases, some of the polarizations gradually vanish except electronic and ionic polarization which caused a rapid decrease in dielectric constant ( $\epsilon'$ ). However, the decline of the dielectric constant value at higher frequency arises for the reason that beyond a definite frequency, the electronic exchange between restricted boundaries cannot follow the alternating field.

The behavior of the dielectric constant also depends on some other features such as dipolar interaction, grain boundaries, and voids [32]. According to Koop's phenomenological theory, structurally dielectric materials are composed of conductive grains that are enclosed within weak resistive grain boundaries. At minimum frequencies, grain restrictions are in control while at maximum frequencies grain boundaries become highly effective for all samples of the  $\text{Bi}_2\text{Se}_3$ . [33]

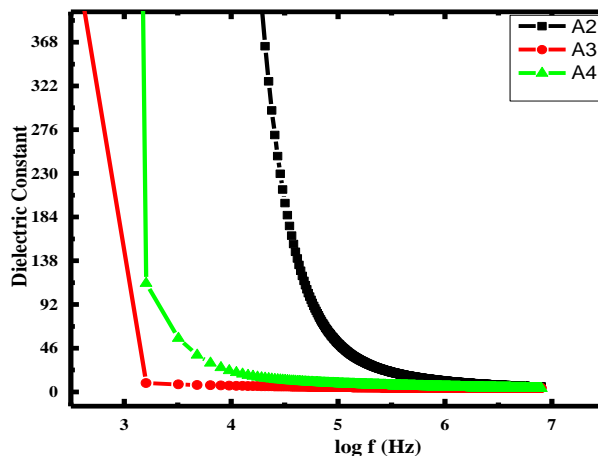


Fig. 5. Variation of dielectric constant ( $\epsilon'$ ) with  $\log F$  at room temperature for the  $\text{Bi}_2\text{Se}_3$  samples.

### 5.2. Dielectric loss ( $\epsilon''$ )

The energy dissipated in dielectric systems due to the movement of charge through the material called dielectric loss. When the AC field is subjected to an imperfection system electric polarization lags behind the alternate current and net electric polarization, which is not in phase with the applied alternate field, thus causing dielectric loss. As polarization is more activated at lower frequencies and thus motivates greater dielectric loss. Just like the dielectric constant, initially, the value of the dielectric loss is higher at lower frequencies thereafter it comes down regularly and ultimately becomes constant, showing customary variation with an increase in frequency.

Fig. 6 shows the behavior of dielectric loss according to frequency for Bismuth Selenide. As it can be seen, at 1 kHz A2 sample has a higher dielectric loss ( $\epsilon''=1.53 \times 10^2$ ) as compared to A4 ( $\epsilon''=2.48$ ) and A3 ( $\epsilon''=1.90$ ) sample respectively. At the frequency 1MHz values of dielectric loss decrease up to  $7 \times 10^{-1}$ ,  $3.20 \times 10^{-1}$  and  $6 \times 10^{-2}$  for the samples A2, A4, and A3 respectively. Similarly, for the frequency at 8 MHz values drop down to  $4.90 \times 10^{-1}$ ,  $2 \times 10^{-1}$  and  $2 \times 10^{-2}$  for the A2, A4, and A3 samples respectively. This revealed that at higher frequencies samples become highly effective for all samples.

As it can be seen in the Fig. 6 the samples (A2) prepared in DMF solvent shows the maximum value of the dielectric loss at a higher frequency as compared for the sample (A4) prepared in a mixed solvent (DMF & Ethanol) and for Ethanol (A3) solvent the dielectric constant is minimum. It is revealed that dielectric loss demonstrates analogous graphical activities as observed for dielectric constant.

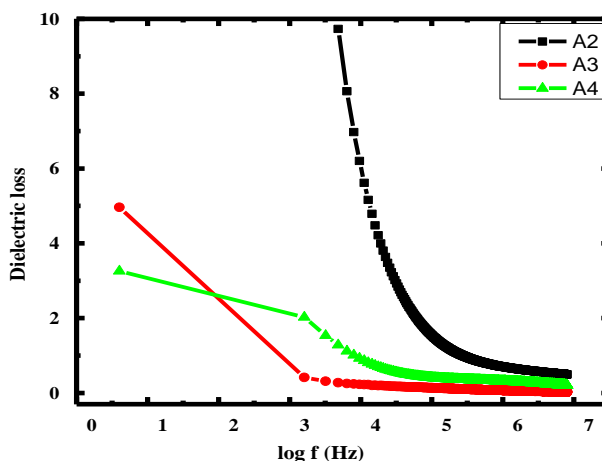


Fig. 6. Frequency dependence of the dielectric loss ( $\epsilon''$ ) of the samples measured at RT.

### 5.3. Tangent loss ( $\tan\delta$ )

Fig. 7, shows the variation of a tangent of the dielectric loss ( $\tan\delta = \epsilon''/\epsilon'$ ) with logarithmic frequency for  $\text{Bi}_2\text{Se}_3$ , which represents energy dissipation under the action of applied alternating fields, and is a more meaningful parameter that quantifies the dielectric loss. Overall, the value of the tangent loss is low up to a frequency 1K Hz and after that graph gradually increases with a rise in frequency and again gradually increase (for sample A2 & A4) with a further increase in frequency [34]. For sample A3, the value of  $\tan\delta$  rapidly increases about 10 kHz of the frequency range and then decreases gradually throughout the frequency range owing to dipolar contribution towards polarization [35]. Also, it is noticed from Table. 6 for sample A2 initially graph remains constant up to 10 kHz then rapidly increases about 10 kHz of the frequency range. The variation of tangent loss ( $\tan\delta$ ) of the A2 and A4 samples shows constant plateau type behavior above 10 kHz of the frequency range. Hence sample A2 shows a less tangent loss ( $5.31 \times 10^{-3}$ ) up to 10 kHz than A4 ( $4.12 \times 10^{-2}$ ) and A3 ( $3.51 \times 10^{-2}$ ).

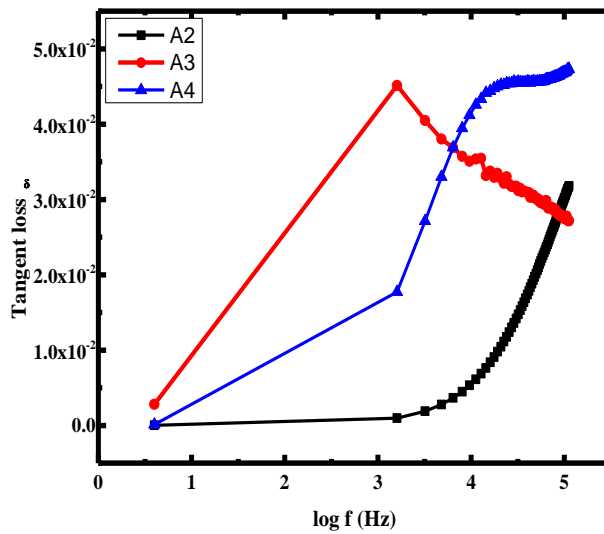


Fig. 7. Shows Frequency dependence of the tangent loss ( $\tan\delta$ ) of the samples measured at RT.

#### 5.4. Impedance study (Z)

Impedance study is a comparatively effective way of describing the electrical properties of materials and setting up a link between microstructures and the electrical properties of the material [36].

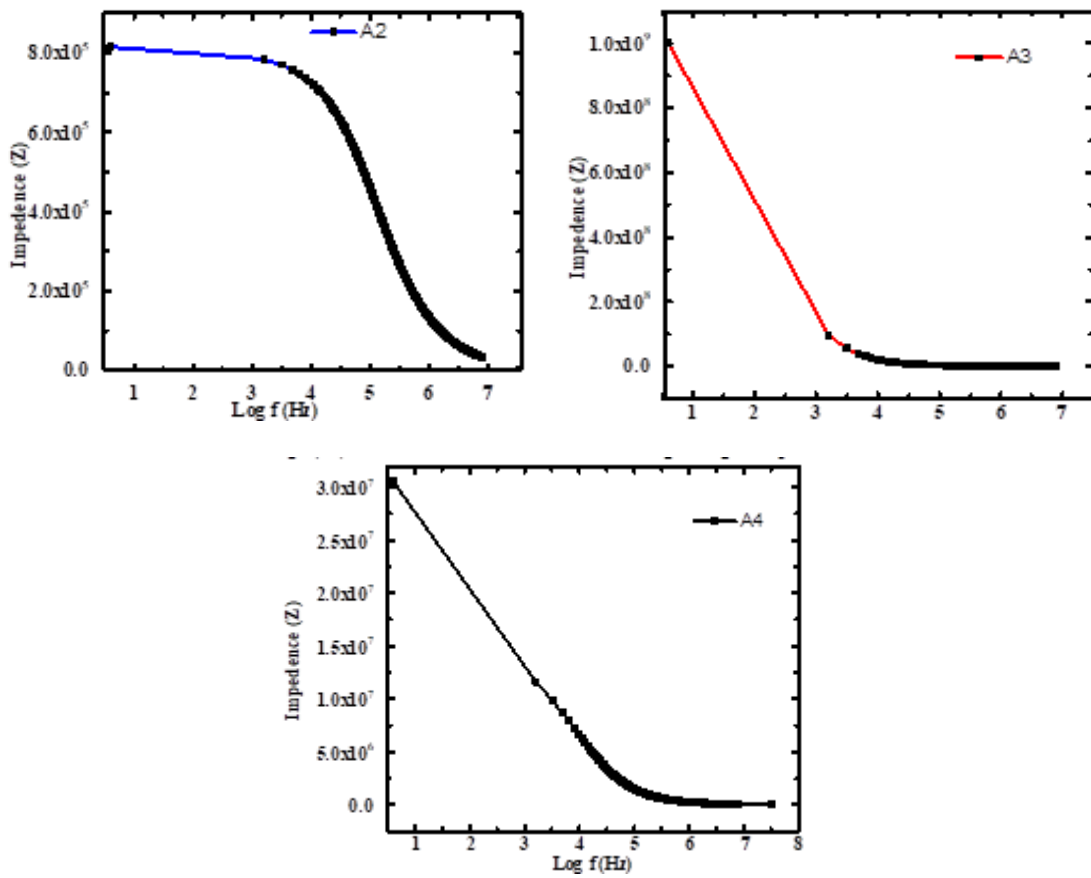


Fig. 8. Variation of impedance (Z) with log f at room temperature for  $\text{Bi}_2\text{Se}_3$  samples.

It is an important tool that measures output response (impedance and ac conductivity) across pressed samples against ac supply. Many materials have grain and grain regions, therefore,

show different physical properties. Fig. 8, shows the variation of impedance values with logarithmic frequency (log F) at room temperature for  $\text{Bi}_2\text{Se}_3$ . It is observed that at minimum frequency, the magnitude of impedance (Z) has a maximum value. As frequency increases the impedance graph gradually comes down and at last all synthesized samples arrived at a stable (constant) value, representing Z is independent of the frequency with analogous behavior. The cause of this variation is that the relaxation time is very short for space charge at higher frequency and space charge recombination is faster which minimizes the space charge polarization that primarily merges the graph.

As it can be seen in Figure 8, the frequency dependence of the Impedance (Z) at room temperature for the  $\text{Bi}_2\text{Se}_3$  of the sample (A4) prepared in a mixed solvent (DMF & Ethanol) shows highest Impedance value than the samples (A3 & A2) prepared in Ethanol solvent and DMF solvent.

## 6. Electrical AC conductivity analysis

The electrical AC conductivity has been calculated by using the following empirical formula:

$$\sigma_{ac} = 2\pi f \epsilon_0 \epsilon' \tan \delta$$

where  $\epsilon_0 = 8.854 \times 10^{-12} \text{ F}\cdot\text{m}^{-1}$  is the vacuum permittivity. According to the above relation, AC conductivity has a direct relation to applied AC frequency and dielectric loss. The dielectric loss is greatly affected by ac conductivity. Fig. 9, shows the behavior of AC electrical conductivity to frequency. As shown in fig. 9, the AC conductivity of the samples is frequency-dependent, therefore, has a lower value at low frequency and increases with the rise in frequency.

Maxwell-Wagner's interfacial model suggests that grain boundaries behave like a potential barrier therefore the charge carriers within grain feel like charges in a potential well. As there is potential restriction between grains, these charge carriers have no access to neighbor grains and these charge carriers can transport freely inside the grains. Due to the small drift velocity of charge carriers inside the grains, there occurs weak conduction at minimum frequencies. As the frequency of the applied field increase, the drift velocity of charge carriers inside the grains becomes strong and charge carriers gain a sufficient amount of energy to go out the restriction boundaries, which results in strong conduction.

The sample prepared in DMF has higher AC conductivity ( $\sigma_{ac}$ ) than the other two solvents representing its potential as a topological insulator.

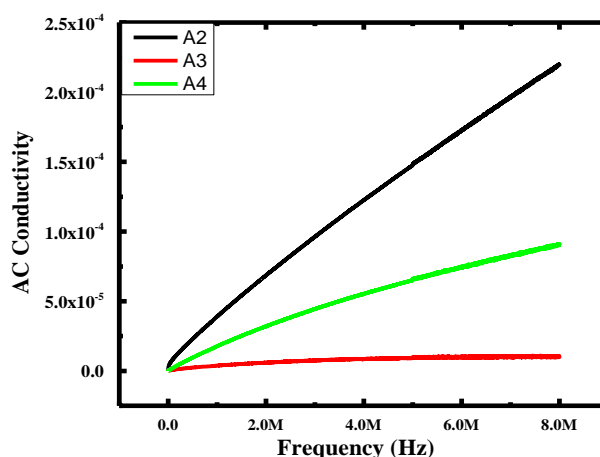


Fig. 9. Presents AC conductivity ( $\sigma_{ac}$ ) comparison for A2, A3 and A4 samples respectively.

## 7. Conclusion

Bismuth Selenide ( $\text{Bi}_2\text{Se}_3$ ) nanopowder has been synthesized via the sol-gel route. The X-ray diffraction pattern (XRD) study of Bismuth Selenide proved the crystalline form and orthorhombic crystal structure. The grain size (G) of Bismuth Selenide calculated in different solvents e.g. DMF, Ethanol, DMF+ Ethanol is 68 nm, 78 nm, and 84 nm respectively. In all synthesized materials prepared in various solvents appeared to be pure  $\text{Bi}_2\text{Se}_3$  products. In the mixed solvent of DMF & ethanol, each solvent bounded with each other more strongly than bismuth and Selenide, so in this mixed solvent, due to weak solubility, the grain size of nanopowder becomes large. FTIR study shows that the wavenumber corresponding to  $680\text{-}800\text{ cm}^{-1}$  represents the vibrational bands of Bismuth Selenide ( $\text{Bi}_2\text{Se}_3$ ). Photoluminescence study of Bismuth Selenide shows the maximum absorption of PL observed at just about 801 nm and the bandgap was approximately 1.7eV for all the solvent. The surface morphology of the synthesized Bismuth Selenide ( $\text{Bi}_2\text{Se}_3$ ) resembled sheet-like micro-crystal morphology. The dielectric study presents dielectric permittivity ( $\epsilon'$ ) and dielectric loss ( $\epsilon''$ ) decreases with the rise in frequency. A tangent loss ( $\tan\delta$ ) shows direct relation with applied frequency. AC conductivity of the samples is frequency-dependent therefore has a lower value at low frequency and increases with a rise in frequency but impedance varies with the inverse of frequency. These studies show that the Bismuth selenide Nanoparticles can be successfully grown by economic and environmental technique Sol-Gel. The dielectric studies showed encouraging results like AC conductivity and Impedance for its application as Topological Insulators.

## References

- [1] M. Z. Hasan and C. L. Kane, Rev. Mod. Phys, vol. 82, p. 3045, 2010; <https://doi.org/10.1103/RevModPhys.82.3045>
- [2] X.-L. Qi and S. C Zhang, Rev. Mod. Phys., vol. 83, p. 1057-1110, 2011; <https://doi.org/10.1103/RevModPhys.83.1057>
- [3] Qi, X.-L.; Zhang, S.-C.; Phys. Today, 2010, 63, 33; <https://doi.org/10.1063/1.3293411>
- [4] Y. Xia, D. Qian, D. Hsieh, L. Wray, A. Pal, H. Lin, A. Bansil, D. Grauer, Y. S. Hor, R. J. Cava and M. Z. Hasan, Nature Physics, vol. 5, p. 398, 2009; <https://doi.org/10.1038/nphys1274>
- [5] Mooser E & Pearson W, Phys Rev B, 101(1956) 492; <https://doi.org/10.1103/PhysRev.101.492>
- [6] Moore, J. & Balents, L., Phys. Rev. B 75, 121306(R) (2007); <https://doi.org/10.1103/PhysRevB.75.121306>
- [7] Hsieh, D. et al., Science 323, 919-922 (2009); <https://doi.org/10.1126/science.1167733>
- [8] Cao, H. L. et al., Phys. Rev. Lett. 108, 216803 (2012); <https://doi.org/10.1103/PhysRevLett.108.216803>
- [9] Chen, X., Ma, X. C., He, K., Jia, J. F. & Xue, Q.K., Adv. Mater. 23, 1162-1165 (2011); <https://doi.org/10.1002/adma.201003855>
- [10] Liu, H. T., Dai, J., Zhang, J. J. & Xiang, W. D., Adv. Mater. Res. 236-238, 1712-1716 (2011); <https://doi.org/10.4028/www.scientific.net/AMR.236-238.1712>
- [11] Hsieh, D. et al., Nature 460, 1101-1105 (2009); <https://doi.org/10.1038/nature08234>
- [12] Giani, Bayaz A. Al, Foucaran A, Pascal - Delannoy F and Boyer A, J. Cryst. Growth, 236 (2002) 217; [https://doi.org/10.1016/S0022-0248\(01\)02095-4](https://doi.org/10.1016/S0022-0248(01)02095-4)
- [13] R. N. Bhattacharya, P. Pramanik, J. Electrochem. Soc. 129 (1982) 332; <https://doi.org/10.1149/1.2123828>
- [14] Bates C W, England L, Appl. Lett, 14 (1996) 390; [https://doi.org/10.1002/1097-0339\(199605\)14:4<390::AID-DC2840140402>3.0.CO;2-5](https://doi.org/10.1002/1097-0339(199605)14:4<390::AID-DC2840140402>3.0.CO;2-5)
- [15] Hyun D. B., Hwang J. S., Oh T. S., Shim J. D., Kolmotes N. V., J. Phys Chem. Solids 59 (1998) 1039; [https://doi.org/10.1016/S0022-3697\(97\)00242-4](https://doi.org/10.1016/S0022-3697(97)00242-4)
- [16] P. Pramanik, R. N. Bhattacharya, A. Mondal, J. Electrochem. Soc. 127 (1980) 1857;

<https://doi.org/10.1149/1.2130017>

- [17] C.W. Bates, L. England, Appl. Phys. Lett. 14 (1996) 390;  
<https://doi.org/10.1063/1.1652701>
- [18] D. B. Hyun, J. S. Hwang, T. S. Oh, J. D. Shim, N. V. Kolomoets, J. Phys. Chem. Solids 59 (1998) 1039; [https://doi.org/10.1016/S0022-3697\(97\)00242-4](https://doi.org/10.1016/S0022-3697(97)00242-4)
- [19] S. Cho et al., Phys. Rev. Lett. 88, 257203 s2002d
- [20] H. Ohno, A. Shen, F. Matsukura, A. Oiwa, A. Endo, S. Katsumoto, and Y. Iye, Appl. Phys. Lett. 69, 363 s1996d; <https://doi.org/10.1063/1.118061>
- [21] Qiu XF, Zhu JJ, Pu L, Shi Y, Zheng YD, Chen HY., Inorg Chem Commun 2004; 7: 319-21; <https://doi.org/10.1016/j.inoche.2003.11.015>
- [22] Cui HM, Liu H, Wang JY, Li X, Han F, Boughton RI., J Cryst Growth 2004; 271: 456-61; <https://doi.org/10.1016/j.jcrysgro.2004.08.015>
- [23] Cui HM, Liu H, Li X, et al., J Solid State Chem 2004; 177: 4001-6; <https://doi.org/10.1016/j.jssc.2004.06.042>
- [24] Wang WZ, Geng Y, Qian YT, Xie Y, Liu XM., Mater Res Bull 1999; 34: 131-4; [https://doi.org/10.1016/S0025-5408\(98\)00203-7](https://doi.org/10.1016/S0025-5408(98)00203-7)
- [25] M. E. Overberg, B. P. Gila, C. R. Abernathy, S. J. Pearton, N. A. Theodoropoulou, K. T. McCarthy, S. B. Arnason, and A. F. Hebard, Appl. Phys. Lett. 79, 3128 s2001d; <https://doi.org/10.1063/1.1416472>
- [26] M. L. Reed, N. A. El-Masry, H. H. Stadelmaier, M. K. Ritums, M. J. Reed, C. A. Parker, J. C. Roberts, and S. M. Bedair Appl. Phys. Lett. 79, 3473 s2001d' <https://doi.org/10.1063/1.1419231>
- [27] V. T. Patil, Y. R. Toda, D. N. Gujarathi "Structural, Transport and Optical Properties of Nanostructured Vacuum Evaporated Bi<sub>2</sub>Se<sub>3</sub> Thin Films" 262936867
- [28] Cosmas M. Muiva,1,2 Charles Moditswe "Chemical Synthesis and Properties of Novel Bi<sub>2</sub>Se<sub>3</sub> Nanostructures and Microplatelets"; <https://doi.org/10.5402/2012/839612>
- [29] K.F. Cai, L. Wang, Phys. D "Synthesis and Characterization of Bi<sub>2</sub>Se<sub>3</sub> Thermoelectric Nanopowders "1874-8465/08
- [30] J.Joy Jeba Vijila, K. Mohan, Phys. D "Microwave-assisted Bi<sub>2</sub>Se<sub>3</sub>nanoparticles using various organic solvents" 153 (2016) 457-464; <https://doi.org/10.1016/j.saa.2015.08.041>
- [31] S. Pattanayak, R.N.P. Choudhary, P. R. Das, J. Mater. Sci.: Mater. Electron., 24 (2013) 2767; <https://doi.org/10.1007/s10854-013-1168-4>
- [32] B.K. Barick, K.K. Mishra, A.K. Arora, R.N.P. Choudhary, Dilip K. Pradhan, J. Phys. D: Appl. Phys., 44 (2011) 355402; <https://doi.org/10.1088/0022-3727/44/35/355402>
- [33] C.G. Koops, On the dispersion of resistivity and dielectric constant of some semiconductors at audio frequencies. Phys. Rev. 83, 121-124 (1951); <https://doi.org/10.1103/PhysRev.83.121>
- [34] R.N.P. Choudhary, Dillip K. Pradhan, C.M. Tirado, G.E. Bonilla, R.S. Katiyar, J. Mater. Sci., 42 (2007) 7423; <https://doi.org/10.1007/s10853-007-1835-z>
- [35] F. Yan, M. On Lie, L. Lu, J. Phys. Chem. C., 114 (2010) 6994; <https://doi.org/10.1021/jp1009127>
- [36] R. Das, T. Sarkar and K. Mandal, J. Phys. D: Appl. Phys., 45 (2012) 455002; <https://doi.org/10.1088/0022-3727/45/45/455002>